Tuning of the ferromagnetic and superconducting transitions by tin-doping in $RuSr_2GdCu_2O_8$

A. C. McLaughlin and J. P. Attfield
Interdisciplinary Research Centre in Superconductivity, University of Cambridge, Madingley Road, Cambridge CB3 0HE, United Kingdom
and Department of Chemistry, University of Cambridge, Lensfield Road, Cambridge CB2 1EW, United Kingdom
(Received 30 July 1999)

Solid solutions $Ru_{1-x}Sn_xSr_2GdCu_2O_8$ with nominal compositions $x=0-0.4$ have been prepared, although some secondary phases are also present. Powder x-ray diffraction and physical measurements show that Sn^{4+} substitutes only at the Ru sites in this layered material. Sn-doping suppresses the ferromagnetic moment in the ruthenate layers, and the Curie temperature decreases from 138 K in the undoped material to 78 K for $x=0.4$. This enhances the conductivity of the CuO_2 planes and the onset of superconductivity increases from 36 K at $x=0$ to 48 K at $x=0.2$, but falls thereafter. This may reflect the increase in hole transfer to the CuO_2 planes and the reduction of ferromagnetic order within the ruthenate layers. [S0163-1829(99)04746-3]

The 1212-type layered cuprate $RuSr_2GdCu_2O_8$ (Refs. 1 and 2) has recently been found to display coexisting ferromagnetism and superconductivity.[3–5] Samples typically have a Curie transition at $T_M=132$ K and bulk superconductivity below $T_C=0-46$ K. A variety of physical measurements, in particular zero-field muon spin rotation experiments,[5] have demonstrated that the material is microscopically uniform with no evidence for spatial phase separation of superconducting and magnetic regions. Superconductivity is associated with the copper oxide planes, while the ruthenium oxide slab behaves like $SrRuO_3$,[6,7] which is an itinerant electron ferromagnet below $T_M=165$ K, rather than Sr_2RuO_4, which is a *p*-wave superconductor with $T_C\approx 1$ K.[8,9] A coexistence of superconductivity and weak ferromagnetism (canted antiferromagnetism) was previously found in the related 1222-type materials $RuSr_2R_{1.4}Ce_{0.6}Cu_2O_{10-\delta}$ ($R=$Gd or Eu).[10]

$RuSr_2GdCu_2O_8$ is found to be oxygen stoichiometric, and the doping of the copper oxide planes necessary to induce superconductivity arises from overlap of the minority spin Ru:t_{2g} and the Cu:$3d_{x^2-y^2}$ bands. The distribution of holes between the two bands may thus be written in terms of average oxidation states as $Ru^{5-2p}Sr_2Gd(Cu^{2+p})_2O_8$. Transport measurements suggest that the copper oxide planes are underdoped with $p\approx 0.1$ holes per Cu atom,[3] although a much higher estimate of $p\approx 0.4$ obtains from bond valence summations based on the refined crystal structure,[4] which is consistent with the properties of the Ru oxide layer. This contradiction suggests that a large proportion of the holes in the copper oxide layers are trapped or strongly scattering by the ferromagnetic Ru moments. To investigate the charge distribution in $RuSr_2GdCu_2O_8$ further, we have attempted to substitute Ru by diamagnetic Sn^{4+}, which is of a similar size and charge. Here we report preliminary results for samples of nominal composition $Ru_{1-x}Sn_xSr_2GdCu_2O_8$ ($x=0,0.1,0.2,0.3,0.4$) which have characterized by powder x-ray diffraction, superconducting quantum interference device (SQUID) magnetometry, and resistivity measurements.

Ceramic samples of the above compositions were prepared by the solid-state reaction of stoichiometric powders of RuO_2, SnO_2, $SrCO_3$, Gd_2O_3, and CuO. These were ground and die pressed into pellets before preliminary reaction in air at 1000 °C for 3 days. The samples were reground, repelleted, and heated at 1050 °C in flowing oxygen for a further 3 days and, finally, slow cooled to room temperature.

Powder x-ray diffraction patterns were recorded at room temperature using Cu $K\alpha$ radiation (Fig. 1). Changes in the peak positions of the tetragonal $RuSr_2GdCu_2O_8$-type phase indicate solid solution formation, but small amounts of the secondary perovskite phases $SrSnO_3$ and $SrRuO_3$ were also seen. The contributions from all three phases were fitted to the x-ray data, using the previously reported model for $RuSr_2GdCu_2O_8$ which uses a split site for the oxygen atoms in the RuO_2 planes to model rotations of RuO_6 octahedra around the *c* axis.[4] (These rotations result from the mismatch of the in-plane Ru-O and Cu-O bonds and have a coherence length that is too small to lead to an observable superstructure in the x-ray diffraction experiment, although this is seen by electron diffraction.[4]) The results in Table I show that substitution of Sn into $RuSr_2GdCu_2O_8$ increases the *a* cell parameter while *c* decreases, although there is no significant change in the cell volume. Refinement of the internal coor-

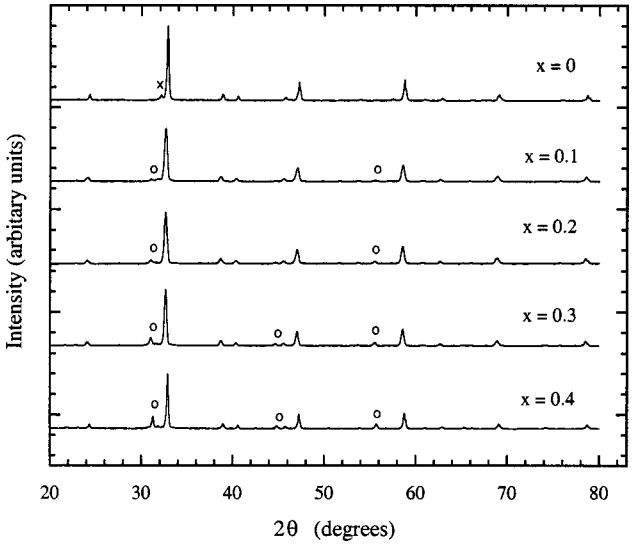

FIG. 1. Powder x-ray diffraction patterns for $Ru_{1-x}Sn_xSr_2GdCu_2O_8$ solid solutions of nominal $x=0-0.4$ with the most intense peaks from the $SrRuO_3$(×) and $SrSnO_3$(○) secondary phases marked.

TABLE I. Tetragonal cell constants and volume, a, c, and V; the remanent moments μ_R, coercive fields H_{CO}, and saturated moments per Ru atom μ_{Ru}, at 10 K; and 250 K resistivities of $Ru_{1-x}Sn_xSr_2GdCu_2O_8$ samples with nominal x values as shown.

x	a (Å)	c (Å)	V (Å^3)	μ_R (μ_B)	H_{CO} (Oe)	μ_{Ru} (μ_B)	ρ250 K (mΩ cm)
0	3.8387(1)	11.5620(4)	170.37(1)	0.115(7)	330(1)	0.91(1)	4.3(1)
0.1	3.8359(1)	11.5609(6)	170.11(1)	0.096(11)	255(1)	0.77(3)	4.5(2)
0.2	3.8375(1)	11.5575(6)	170.21(1)	0.067(2)	230(1)	0.48(2)	2.0(1)
0.3	3.8379(1)	11.5552(6)	170.21(1)	0.044(1)	160(1)	0.43(5)	2.3(2)
0.4	3.8396(1)	11.5525(6)	170.31(1)	0.030(1)	120(1)	0.30(7)	3.4(1)

dinates shows an increase in the in-plane Ru-O distance and a concomitant decrease in the Ru-O-Ru angle (Fig. 2). This is consistent with substitution of Sn at the Ru sites, as Sn^{4+} is slightly larger than Ru^{4+}/Ru^{5+}. No significant trends in the other Ru-O or Cu-O bond lengths were found.

The magnetizations of the five powdered $Ru_{1-x}Sn_xSr_2GdCu_2O_8$ samples (Fig. 3) were measured on a Quantum Design SQUID magnetometer. Samples were zero field cooled and measured from 10 to 300 K in an applied field of 1 kOe. A broadening of the magnetic transition and a reduction in the Curie temperature T_M with increasing Sn substitution is clearly seen in these data, and the values of T_M (estimated from the minima in dM/dT) are plotted against nominal x in Fig. 4. No Meissner effect is observed below T_c for these powdered samples as the small negative magnetization resulting from intragranular supercurrents is swamped by the positive contributions from the ferromagnetic Ru and paramagnetic Gd moments.

Magnetic hysteresis loops recorded at 10 K with the field swept between ± 50 kOe confirm the ferromagnetic order in all the samples; a typical loop is shown in Fig. 5. A very small hysteresis was observed for each sample, and the coercive fields and remanent moments are displayed in Table I: these both decrease rapidly with x. Both the ferromagnetic Ru moment μ_{Ru} and paramagnetic Gd moments μ_{Gd} contribute to the overall magnetization. The saturated Ru moment was estimated by fitting the total magnetic moment in the range $H = 25-50$ kOe with the function

$$\mu(H) = \mu_{Gd} F(H) + (1-x)\mu_{Ru},$$

where $F(H)$ is the Brillouin function for the $S = 7/2$ Gd^{3+} spins. The estimated Ru moment decreases rapidly with x as shown in Table I.

The resistivities of sintered polycrystalline bars (approximate dimensions $4 \times 4 \times 12$ mm^3) were measured between 15 and 300 K using the standard four-probe ac technique (Fig. 6). Broad superconducting transitions are observed in all five $Ru_{1-x}Sn_xSr_2GdCu_2O_8$ samples, although the zero-resistance point lies below the lowest measured temperature for some samples. The onset T_c (defined by the temperature of the resistivity maximum) is plotted against x in Fig. 3. All five samples are semiconducting ($d\rho/dT < 0$) above T_c; however, the $x = 0.2$ sample changes to metallic ($d\rho/dT > 0$) behavior above 220 K. This sample has the highest T_c and the lowest normal-state resistivity (Table I).

The systematic changes in the crystallographic, magnetic, and resistive properties of the $Ru_{1-x}Sn_xSr_2GdCu_2O_8$ samples show that Sn is progressively replacing Ru in the primary phase. The observation of a superconducting transition even in the $x = 0.4$ sample demonstrates that no significant Sn substitution occurs at the Cu sites, as the superconductivity in this material[5] and other cuprates is sensitive to very small levels of such diamagnetic dopants. The presence of the secondary phase $SrSnO_3$ indicates that the actual levels of Sn substitution are lower than the nominal proportions quoted.

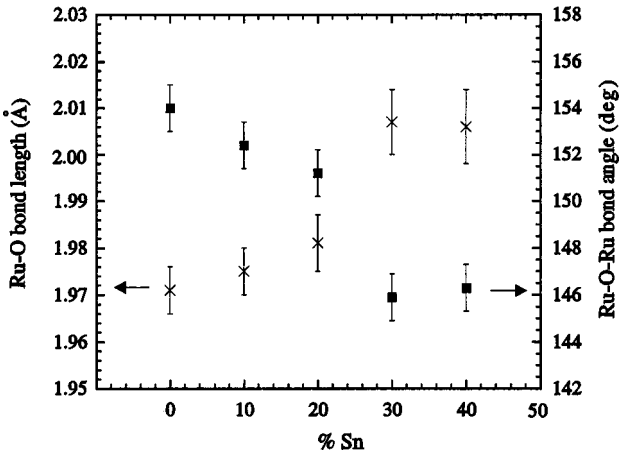

FIG. 2. Changes in the xy-plane Ru-O bond length and Ru-O-Ru angle with nominal Sn content in $Ru_{1-x}Sn_xSr_2GdCu_2O_8$ solid solutions.

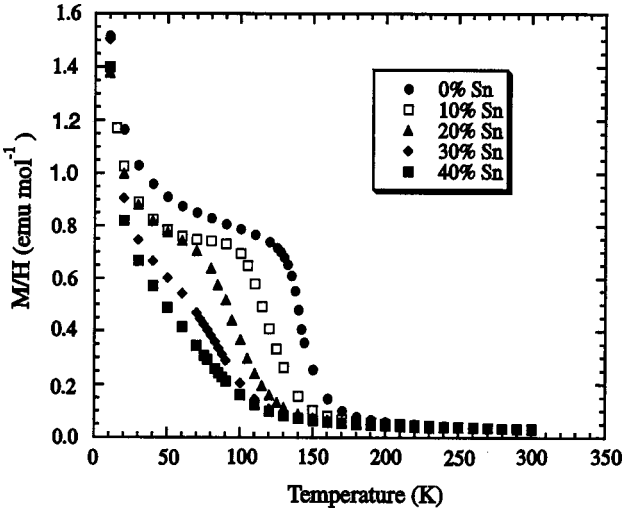

FIG. 3. Magnetization/field data for the $Ru_{1-x}Sn_xSr_2GdCu_2O_8$ solid solutions.

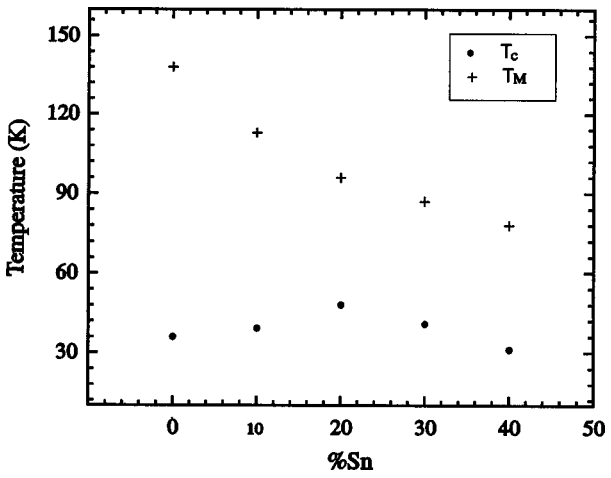

FIG. 4. Variation of the Curie temperature T_M and the onset superconducting critical temperature T_c with nominal Sn content in $Ru_{1-x}Sn_xSr_2GdCu_2O_8$ solid solutions.

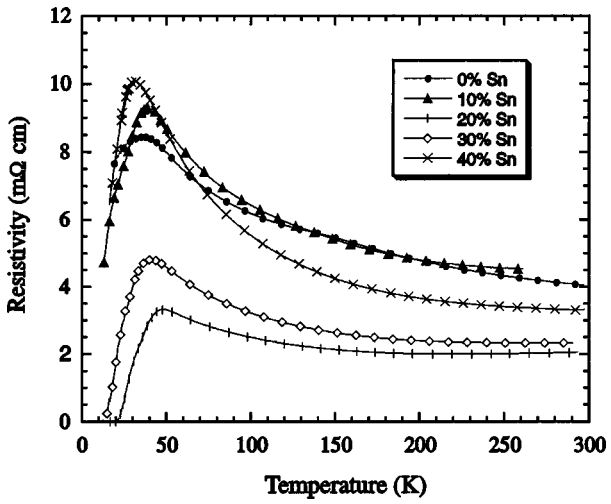

FIG. 6. Resistivity data for polycrystalline $Ru_{1-x}Sn_xSr_2GdCu_2O_8$ solid solutions.

However, $SrSnO_3$ is diamagnetic and nonconducting, and the ferromagnetic conducting perovskite $SrRuO_3$ is present at $<3\%$ levels in all the doped samples, so that the bulk physical measurements reported here reflect the properties of the majority $Ru_{1-x}Sn_xSr_2GdCu_2O_8$ phases.

Sn^{4+} is diamagnetic and does not contribute electronic states close to the Fermi level in the $Ru_{1-x}Sn_xSr_2GdCu_2O_8$ solid solutions. This disrupts the itinerant electron ferromagnetism of the RuO_2 planes, leading to a rapid decrease in T_M from 138 to 78 K at $x=0.4$. The substitution also affects the electronic properties of the CuO_2 planes. The hole distribution may now be written $(Ru^{5-2p})_{1-x}Sn_xSr_2Gd(Cu^{2+p+x(0.5-p)})_2O_8$, showing that the hole concentration in the CuO_2 planes increases with Sn doping x if the intrinsic doping level p remains constant. This is consistent with the initial trend in the resistivity data for $x=0-0.2$, as T_c increases and the normal-state resistivity decreases and becomes more metallic in character. However, the subsequent fall in T_c for $x=0.3$ and 0.4 is not as expected for overdoped materials, as the normal-state resistivities should become more metal-like, whereas the observed variations (Fig. 6) show a return to semiconducting behavior. This may reflect the presence of increasing amounts of nonconducting $SrSnO_3$ within these polyphasic sintered ceramic samples. These results are in contrast to previous substitutions of 10% Y at the Gd site, which change T_M and T_c by <5 K and of 3% Zn for Cu, which suppresses superconductivity, but leaves T_M unchanged.[5]

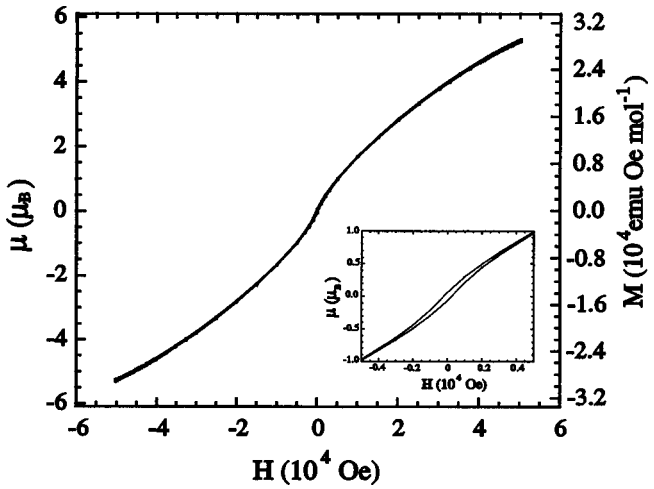

FIG. 5. Magnetic hysteresis loop for $Ru_{0.8}Sn_{0.2}Sr_2GdCu_2O_8$ at 10 K. The inset shows the small hysteresis.

The coexistence of ferromagnetism and superconductivity in $RuSr_2GdCu_2O_8$ has previously been attributed to the momenta of the Cooper pairs in the CuO_2 planes and the ferromagnetic moments in the RuO_2 planes both being parallel to the xy plane.[3,5] However, the relatively low T_c and the disparity between the apparent hole concentration inferred from transport measurements and that estimated by bond valence summations suggested some hole trapping or scattering in the normal state and pair breaking within the superconducting state of the CuO_2 planes is caused by the ferromagnetism. This could result from slight canting of the moments due to disorder of the rotations and tilts of the RuO_6 octahedra or the presence of out-of-plane spin waves. This view is supported by the increases in conductivity and superconductivity with initial Sn doping as the ferromagnetic Ru moment decreases.

In conclusion, this study shows that Sn can be substituted for Ru in the ferromagnetic superconductor $RuSr_2GdCu_2O_8$, enabling the Curie temperature to be reduced from 138 to 78 K, while the onset of the superconducting transition initially increases from 36 to 48 K. The latter change may reflect an increase in the hole doping of the CuO_2 planes, the suppression of the ferromagnetism, or both of these factors. The ability of Sn substitution to tune both electronic transitions over large temperature ranges and the use of ^{119}Sn as an NMR and Mösshauer nucleus will enable the unique coexistence of high-temperature ferromagnetism and superconductivity in this system to be investigated further, after phase-pure $Ru_{1-x}Sn_xSr_2GdCu_2O_8$ solid solutions have been prepared.

We thank EPSRC for the provision of research Grant No. GR/M59976 and S. Rycroft for help with resistivity measurements.

[1] L. Bauernfeind, W. Widder, and H. F. Braun, Physica C **254**, 151 (1995).
[2] I. Felner, U. Asaf, S. Reich, and Y. Tsabba, Physica C **311**, 163 (1999).
[3] J. L. Tallon, C. Bernhard, M. E. Bowden, P. W. Gilbert, T. M. Stoto, and D. J. Pringle, IEEE Trans. Appl. Supercond. **9**, 1696 (1999).
[4] A. C. Mclaughlin, W. Zhou, J. P. Attfield, A. N. Fitch, and J. L. Tallon, Phys. Rev. B **60**, 7512 (1999).
[5] C. Bernhard, J. L. Tallon, Ch. Niedermayer, Th. Blasius, A. Golnik, E. Brucher, R. K. Kremer, D. R. Noakes, C. E. Stronach, and E. J. Ansaldo, Phys. Rev. B **59**, 14 099 (1999).
[6] J. M. Longo, P. M. Raccah, and J. B. Goodenough, J. Appl. Phys. **39**, 1327 (1968).
[7] S. Uchida, Physica C **185-189**, 28 (1991).
[8] Y. Maeno, H. Hashimoto, K. Yoshida, S. Nishizaki, T. Fujita, J. G. Bednorz, and F. Lichtenberg, Nature (London) **372**, 532 (1994).
[9] K. Ishida, H. Mukuda, Y. Kitaoka, K. Asayama, Z. Q. Mao, Y. Mori, and Y. Maeno, Nature (London) **396**, 658 (1998).
[10] I. Felner, U. Asaf, Y. Levi, and O. Millo, Phys. Rev. B **55**, R3374 (1997).